ROYAL SOCIETY OPEN SCIENCE

royalsocietypublishing.org/journal/rsos

Research

Cite this article: Sakthivel T, Kluge T, Ghosh P, Stein D. 2026 Laser spectroscopy-based oxygen and clumped isotope acid fractionation factors using two different carbonate digestion techniques. *R. Soc. Open Sci.* **13**: 251320.
https://doi.org/10.1098/rsos.251320

Received: 4 August 2025
Accepted: 26 February 2026

Subject Category:
Chemistry

Subject Areas:
analytical chemistry, geochemistry, spectroscopy

Keywords:
infrared spectrometer, stable and clumped isotopes, acid fractionation factor, calcite, data reduction methods

Author for correspondence:
Prosenjit Ghosh
e-mail: pghosh@iisc.ac.in

Laser spectroscopy-based oxygen and clumped isotope acid fractionation factors using two different carbonate digestion techniques

Thamizharasan Sakthivel[1,2], Tobias Kluge[3,4], Prosenjit Ghosh[1,2] and Dorothea Stein[3,4]

[1]Centre for Earth Sciences, and [2]Divecha Centre for Climate Change, Indian Institute of Science, Bengaluru, Karnataka, India
[3]Institute for Applied Geosciences, and [4]Laboratory for Environmental and Raw Material Analysis (LURA), Karlsruhe Institute of Technology, Karlsruhe, Baden-Württemberg, Germany

PG, 0000-0001-7828-577X

The Aerodyne tunable infrared laser differential absorption spectrometer (TILDAS) measures stable oxygen (δ_{628}) and clumped (Δ_{638}) isotopes in carbonates, analysing infrared absorbance of CO_2 isotopologues produced during phosphoric acid digestion. These isotopes are influenced by acid fractionation, which varies with both digestion temperature and technique, making it essential to quantify the fractionation factor for data comparability and to assess isotopic exchange between the product CO_2 and H_2O. Here, we present analysis of Carrara Marble (MAR-J1) calcite, the same as primary standard NBS19 reacting with approximately 104% phosphoric acid at varying temperatures via two traditional digestion techniques: (i) break seal (BS)/McCrea-type digestion technique, which allows a complete equilibration between product CO_2 and H_2O; and (ii) individual acid bath (IAB) technique, which compromises the equilibration process. Our experiments reveal that the calcite acid fractionation for δ_{628} and Δ_{638} varies with digestion technique because CO_2–acid contact time controls exchange with H_2O. The IAB technique yields a shallower slope for δ_{628} and a steeper slope for Δ_{638}, indicating minimal isotopic resetting, whereas the BS technique exhibits the opposite pattern, suggesting enhanced isotopic exchange during

THE ROYAL SOCIETY PUBLISHING

extended CO_2–acid interaction. These findings facilitate robust inter-laboratory comparisons of δ_{628} and Δ_{638} ratios in calcite.

1. Introduction

Stable oxygen ($\delta^{18}O$) and clumped isotope values (Δ_{47}) in carbonates are widely used as geothermometers [1–9], essential for reconstructing past climate information [10–16], palaeo-elevation [17,18], thermal history of rock [19,20] and diagenetic imprints [21]. The isotopic analysis is typically performed on CO_2 produced by the digestion of carbonate with greater than 100% phosphoric acid (H_3PO_4) at a constant temperature using a gas source isotope ratio mass spectrometer (IRMS) [1,4,9,22–24]. The approach used for stable isotope analysis involves standard-sample bracketing using dual-inlet peripherals or a continuous flow mode. The more common practice for clumped isotope analysis uses a dual inlet peripheral for the sample and working reference gas (WRG) introduction and integrates observation for a long duration to build counting statistics for high-precision measurements using IRMS. This task imposes a significant challenge for analysis, which includes long machine times of 2–4 hours per sample and the requirement for carbonate samples to yield more than 30 µmol of CO_2 [4–6,25,26]. Additionally, the data reduction process for establishing the abundances of isotopologues of CO_2, specifically masses 46 ($^{18}O^{12}C^{16}O$, $^{17}O^{13}C^{16}O$, $^{17}O^{12}C^{17}O$) and 47 ($^{18}O^{13}C^{16}O$, $^{17}O^{13}C^{18}O$, $^{17}O^{13}C^{17}O$) requires correction for ^{17}O excess to define $\delta^{18}O$ and Δ_{47} values. The ^{17}O interference is taken into account by incorporating the correction factor, which assumes a mass-dependent relationship between ^{17}O and ^{18}O ($\lambda = 0.528$; where $\lambda = \ln(\delta^{17}O+1)/\ln(\delta^{18}O+1)$) [27–29]. However, natural samples often deviate from this assumed relationship, introducing significant uncertainty in both $\delta^{18}O$ and Δ_{47} observations [30].

The introduction of cavity ring-down spectroscopy and tunable infrared laser differential absorption spectrometer (TILDAS) allows the determination of infrared absorbance for the abundance of different CO_2 isotopologues without any interference from mass ^{17}O [31–36]. The versatility of TILDAS is used for simultaneous analysis of $\delta^{18}O$ and Δ_{47} of CO_2 liberated from carbonate with acid digestion at the precision of 0.08‰ and 0.01‰, respectively [32].

The temperature effect on acid-carbonate digestion is one of the most critical factors for the measurement of $\delta^{18}O$ and Δ_{47} isotopic composition of carbonates. Traditionally, these isotopes are measured in CO_2 evolved from the digestion of carbonate with greater than 100% phosphoric acid (H_3PO_4) at 25°C, with a complete digestion duration of 18–24 hours [1,4,22–24,37–39],

$$CaCO_3 + H_3PO_4 \rightleftharpoons CaHPO_4 + CO_2 + H_2O\,. \tag{1.1}$$

During carbonate-acid digestion, only two-thirds of the oxygen in the carbonate lattice is liberated in the product CO_2, while the remaining one-third is allocated to the product H_2O. The $\delta^{18}O$ fractionation between carbonate and CO_2 is determined experimentally by multiple works following the same approach proposed by Sharma & Clayton [40], but using different calcite reference materials with widely different major elements bulk isotopic composition, later validated theoretically [2,40–42]. The different observations suggest a range in fractionation for $\delta^{18}O$ by 10.20–10.72‰ between product CO_2 and carbonate at the acid-digestion temperature of 25°C. This approach was extended to clumped isotope investigation at 25°C acid-digestion temperature using both experimental and theoretical approaches, with fractionation of 0.20–0.22‰ between product CO_2 and synthesized carbonate at high-pressure and temperature conditions [4,41].

High sample throughput was achieved both in $\delta^{18}O$ and Δ_{47} isotope communities by digesting the carbonate with acid at 70°C [7,43,44] and 90°C [5,6]. These high-temperature digestion isotope values have to be corrected for acid fractionation using the equations

$$1000\ln\alpha^{18}_{\text{dig.temp}-25^\circ\text{C}} = 1000\left(\frac{\delta^{18}O_{\text{dig.temp}} - \delta^{18}O_{25^\circ\text{C}}}{\delta^{18}O_{25^\circ\text{C}} - 1000}\right), \tag{1.2}$$

$$1000\ln\alpha^{47}_{\text{dig.temp}-25^\circ\text{C}} = 1000\left(\frac{\Delta_{47\text{ at dig.temp}} - \Delta_{47\text{ at }25^\circ C}}{\Delta_{47\text{ at }25^\circ C} - 1000}\right), \tag{1.3}$$

to compare their values with acid digestions at 25°C. This is necessary because the primary standard for carbonate stable isotope NBS-19 value has been reported based on acid-carbonate digestion at 25°C [23,45]. The initial experimental Δ_{47}-isotope thermometry calibrations [4,9,46] and the theoretical calibration [3] were produced based on acid-carbonate digestion at 25°C. Additionally, for solid-state

reordering experiments, the theoretical calibration based on 25°C acid-carbonate digestion is used to estimate the equilibrium Δ_{47} value, aiding in understanding reaction kinetics by measuring the offset between apparent and equilibrium Δ_{47} [19]. This brought consistency between experimental and theoretical observations [47].

In most cases, high-temperature digestion (at 90 and 70°C) is conducted using three methods: common acid bath (CAB) [8,48,49], individual acid bath (IAB) [5,6] and acid drip method [7,43,44]. Meanwhile, low-temperature digestion was performed either in a McCrea-type reaction chamber [4] or in a modified form known as a sealed vessel [48,49] or through the break seal (BS) method [25]. To better understand acid fractionation, numerous studies have been conducted aiming to investigate various aspects, including the variation in mineralogy [8,41,48,50,51], cation substitution in carbonates [52], the volume of the reaction chamber [48], the technique of acid-carbonate digestion [22,48,49] and the water vapour pressure over the acid [8,53].

The previous investigation of $\delta^{18}O$ and Δ_{47}-specific acid fractionation in calcite, conducted at various temperatures, has revealed a diverse relationship between isotope fractionation and acid temperature for sealed vessels and the CAB method [48,49]. This variation arises from factors including the duration of CO_2 and H_2O isotopic exchange, the method of CO_2 extraction and the volume of the reaction chamber [48,49]. The CAB method-based acid fractionation is used to correct data obtained using the IAB [5] and acid drip methods [43]. However, a drawback of the CAB method is its use of the same acid for multiple samples, resulting in a memory effect on isotope values [49]. Additionally, there is a lack of information regarding how the density and pH of phosphoric acid change during subsequent carbonate digestion using the same acid. During carbonate-acid digestion, the H^+ in the phosphoric acid is consumed to produce H_2O and CO_2 from carbonate, which, upon degassing, will lead to an increment in the acid's pH. Conversely, this process differs from the IAB and acid drip methods, where new acid is introduced in the reaction chamber for each carbonate digestion. It is important to note that previous isotope acid fractionation experiments analysed the CO_2 using IRMS. However, an acid fractionation factor for carbonate-derived CO_2 across varying acid digestion temperatures, analysed using TILDAS, has yet to be established.

In this study, we present the first oxygen and clumped isotope acid fractionation data for calcite across varying acid digestion temperatures, analysed using TILDAS. We applied two distinct acid-carbonate digestion techniques: the BS and the IAB methods. Furthermore, we provide accuracy and reproducibility of TILDAS measurements by reporting multiple replicate analyses on six inter-laboratory carbonate reference materials.

2. Material and methods

2.1. Carbonate material and experimental conditions

In this study, we examined MAR-J1 calcite (less than 250 µm grain size) reference carbonate powder for the establishment of the relationship of acid fractionation factor with temperature of carbonate digestion for simultaneous analysis of stable oxygen and clumped isotopes. MAR-J1 calcite's stable and clumped isotope composition resembles that of NBS-19, a primary standard recommended for carbonate-stable isotope analysis [4,22,25,54]. The resemblance of major and minor element composition of MAR-J1 calcite with NBS-19 is documented, with an average $CaCO_3$ content of 98.0 wt% and approximately 2.0 wt% of $MgCO_3$, along with the presence of minor elements Al, Fe, Cu, Mn, Na and K of less than 0.1% [22]. This makes MAR-J1 an alternative carbonate powder to NBS-19 with similar chemical behavior during acid digestion.

In this study, we conducted experiments with MAR-J1 calcite powder, subjecting it to digestion with 104% phosphoric acid involving two different acid-carbonate reaction methods with different temperatures: (i) BS method at temperatures of 13, 25, 38 and 70°C; and (ii) IAB at temperatures of 50, 70 and 90°C. The concentration of phosphoric acid is maintained rigorously, and its density is monitored intermittently with a constant value of 1.91 g cm^{-3}, which corresponds to 104% of the acid concentration. This is done with the aid of a density meter (Anton Paar DMA 35 portable density meter). To convert acid densities to acid concentrations, the equation proposed earlier was used [22]. In the description, phosphoric acid stands at 104% in concentration unless otherwise mentioned.

2.2. Acid digestion techniques

2.2.1. Break seal method

The break seal vessel method is a modified version of the McCrea-type vessel recently introduced for stable and clumped isotope analysis [25] (figure 1a). The advantages of the break seal vessel method include: (i) enabling acid-carbonate reactions at 25°C, discounting the offset introduced for acid fractionation in stable isotope analysis, justifying its anchor with primary standard NBS-19 calibration and assignment of values following the identical treatment of carbonate powder [23]; and (ii) ensuring airtight sealing for long storage with no leak [25,50]. Moreover, stable and clumped isotope values of NBS-19 measured using the BS method are consistent with those obtained using both the McCrea-type and sealed vessel methods [25].

The operation of the BS method for acid-carbonate reaction involves two entities: (i) a bottom-sealed cylindrical Pyrex tube (hereafter referred to as the reaction chamber); and (ii) a carbonate powder enclosure (hereafter referred to as the sample holder). Dimensionally, the reaction tube is configured with a 25 cm tube length and segmented into two parts: an upper 15 cm open-end tube with 1 mm wall thickness and 6 mm outer diameter fused to a lower 10 cm tube, which is closed at the bottom with an outer diameter of 9 mm to accommodate the sample holder that rests on the wall of the closed bottom of the reaction chamber (figure 1a). The sample holder is 5 cm in length, prepared from glass tube with a 0.5 mm wall thickness and 3 mm outer diameter, and it is closed at one end (figure 1a).

Approximately 8–10 mg of carbonate powder is transferred into the sample holder upon weighing in a high-precision balance (Sartorius BT 224 S Balance) and placed within a reaction chamber containing 1 ml of orthophosphoric acid. The acid was transferred to the reaction chamber from a bottle storage reservoir using a volumetric Pasteur pipette. Subsequently, the entire set-up loaded with carbonate powder and acid is evacuated to a pressure level of 10^{-3} bar using a peripheral glass extraction line coupled to an Edwards rotary pump (RV12) and flame-sealed 2 cm below the Cajon connector (figure 1a).

Following the sealing step, the sealed reaction chamber is placed inside a water bath maintained at the assigned reaction temperature (±0.1°C). To commence the reaction, the reaction chamber is vigorously shaken so that the carbonate powder can react with the phosphoric acid. The different reaction times for the experiments conducted at constant water bath temperatures of 13, 25, 38 and 70°C are 72, 24, 12 and 4 hours, respectively. Upon completion of the reaction, the reaction chamber is removed from the water bath, and it is processed for the extraction of CO_2 and cleaning using a cryogenic protocol.

2.2.2. Individual acid bath

An IAB is a specially designed reaction vessel fabricated similarly to a CAB, except with a provision to replace the acid for each sample, which discounts the possibility of any memory effect from acid storage involved in the analysis of the CAB (figure 1b) [5,6]. The design of the reaction vessel is a modification of an Erlenmeyer flask of 40 ml volume with an inlet placed horizontally for loading carbonate powders (figure 1b).

The procedure of loading samples involves filling the reaction vessel with 1 ml of phosphoric acid, which is connected to the CO_2 extraction and cleaning line. The reaction vessel is heated to a designated temperature for a duration of 10 min. Approximately 12 mg of reference carbonate powder is loaded into a Pyrex boat, which is placed in the horizontal inlet. The inlet is subsequently sealed from one side using a blind fitted with an ultra-torr. The reaction vessel containing the carbonate powder and phosphoric acid is evacuated for 18 min, which is assigned based on the attainment of a final pressure value of 10^{-1} to 10^{-2} mbar, which varies depending on the acid temperature and modulates the acid-vapour pressure inside the reaction vessel.

The process of evacuation is followed by an acid-carbonate digestion, which is performed after disconnecting the reaction vessel from the Agilent scroll pump (IDP-15), which is devoid of any oil. Carbonate powder is allowed to react with phosphoric acid by dropping the Pyrex boat with the help of a magnet. The reaction temperature is maintained in the reaction vessel with the help of a temperature sensor in the heated aluminium enclosure surrounding the reaction vessel and a magnetic stirrer that ensures the mixing of the acid in contact with the carbonate powder. The product generated during the reaction (CO_2 and H_2O) is cryogenically trapped simultaneously with the help of U-trap

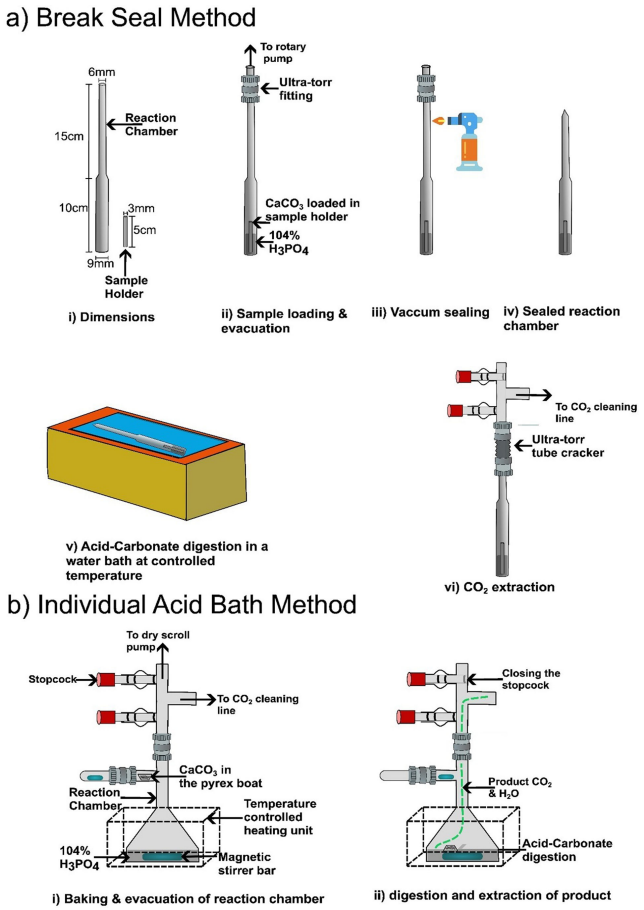

Figure 1. Schematic representations of reaction set-ups used in acid-carbonate digestion with 104% phosphoric acid for the analysis of carbonate-$\delta^{18}O$ and Δ_{47} isotopes. The illustrations show the sample preparation and CO_2 extraction steps for (a) the BS method and (b) the IAB method.

placed close to the reaction vessel (marked as trap 1) (figure 2). The reaction times assigned for complete digestion of carbonate in acid at 50, 70 and 90°C are 60, 30 and 10 min, respectively.

2.3. CO_2 extraction and cleaning

In the case of the IAB method, the CO_2 and H_2O from the acid-carbonate reaction are cryogenically trapped immediately using the U-trap (1st) placed in proximity to the reaction chamber (figure 2). In the case of the BS method, the sealed portion of the reaction chamber is fitted into the ultra-torr union arranged with a tube cracker assemblage. Upon evacuation of the entire set-up to the background pressure of 10^{-3} bar, the broken seal is cracked open, and CO_2 and H_2O are cryogenically trapped in a U-trap (1st) similar to the IAB method (figure 2). Non-condensable gases present in the reaction chambers are evacuated. CO_2 is selectively transferred to the 2nd U-trap using a liquid nitrogen and ethanol mixture (−80°C) in the 1st U-trap, and keeping the liquid nitrogen in the 2nd U-trap. The volume of the 2nd U-trap is independently ascertained with known volume and a LEX 1 Keller gauge, which reads pressure (figure 2). The pressure reading of the CO_2 generated from the acid-carbonate reaction is used for estimation of yield. The CO_2 is afterwards entrained through a stainless steel (SS) U-trap filled with Porapak Q (filled length: 13 cm; inner diameter: 8 mm; volume: 6.5 ml) held at −35°C, and the CO_2 is simultaneously collected in a 3rd U-trap held at liquid nitrogen temperature for assigned elution time of 32 min (figure 2).

The cleaned CO_2 obtained at this step is transferred to the 4th U-trap, which is connected to a 0.75 l SS canister (Festo CRVZS) using a ball valve (Dk-Lok) (figure 2). The SS canister is pre-filled with a specific amount of N_2 (99.999% purity) to achieve a mixing ratio of 0.35% when added to the cleaned CO_2. The CO_2 and N_2 mixture equilibrate for at least 12 hours for the determination of the isotopic composition of CO_2 [55].

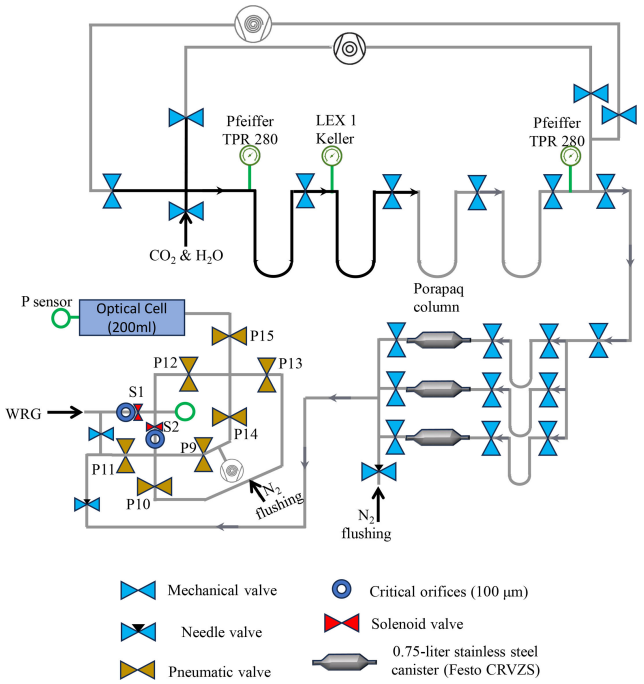

Figure 2. Schematic of the CO_2 cleaning and analysis system. The system includes a CO_2 purification section, a sample collection, mixing and delivery subsystem, and an inlet for spectroscopic analysis. P sensor, pressure sensor; N_2, nitrogen gas; WRG, working reference gas; concentric circles, critical orifice. Black lines represent the glass tubing of the system, while grey lines indicate the stainless steel (SS) tubing.

2.4. Tunable infrared laser differential absorption spectrometer measurements

2.4.1. Isotopic notation for tunable infrared laser differential absorption spectrometer analysis

For TILDAS measurements of CO_2 isotopologues, a laser-specific notation has been adopted by the community [32,33,55], derived from the high-resolution transmission molecular absorption database [56]. In this notation, isotopologues are identified using the second digit of the atomic mass of the atoms involved. For instance, isotopologues like $^{16}O^{12}C^{16}O$, $^{16}O^{13}C^{16}O$, $^{16}O^{12}C^{18}O$ and $^{16}O^{13}C^{18}O$ are denoted as 626, 636, 628 and 638, respectively.

The isotopic composition of isotopologues substituted with a single heavier isotope is expressed as

$$\delta_i = \left(\frac{\frac{[i_{\text{sample}}]}{[626_{\text{sample}}]}}{\frac{[i_{\text{standard}}]}{[626_{\text{standard}}]}} - 1 \right) \times 1000, \tag{2.1}$$

where i represents isotopologues of interest, the TILDAS isotopic ratios δ_{636} and δ_{628} are used as good approximations of the $\delta^{13}C$ and $\delta^{18}O$ notations for IRMS [32,33]. Additionally, δ_{638} approximates the sum of δ_{636} and δ_{628}, and thus represents the combined isotopic ratio, akin to δ_{47}, which is used in IRMS data evaluation [32,33,47]

In the context of clumped isotopes, the variable Δ_i describes the abundance of isotopologues of interest i relative to the expected stochastic distribution of isotopologues:

$$\Delta_i = \left(\frac{R_{i-e}}{R_{i-r}} - 1 \right) \times 1000, \tag{2.2}$$

where $R_{i\text{-}e}$ is the abundance ratio of isotopologue 638 relative to 626 and $R_{i\text{-}r}$ refers to the random distribution condition [33,57].

2.4.2. Tunable infrared laser differential absorption spectrometer configuration and measurement protocol

The TILDAS instrument is a state-of-the-art dual-laser spectrometer, leveraging advanced technology from Aerodyne's commercial atmospheric CO_2 stable isotope analyser [58,59] and an innovative CO_2-clumped isotope prototype [34,35]. The TILDAS instrument uses two quantum cascade lasers

to comprehensively cover the spectral regions of four isotopologues of CO_2 (626, 636, 628 and 638) without negligible-low absorption peak interference at the relevant peaks, enabling simultaneous isotope measurements [33]. An interband cascade laser (laser 1, Nanoplus, Germany) is precisely tuned for 2250.2 cm^{-1} to detect 636 and 638 isotopologues, while a quantum cascade laser (laser 2, Alpes Laser, Switzerland) is tuned for 2285.1 cm^{-1} to detect 626 and 628 isotopologues [33]. The description of the laser system and technical details are available elsewhere [33,58].

Similar to the dual-inlet method for IRMS measurement, a WRG is assigned as an anchor, whose value is independently ascertained using primary standards and also monitored frequently to determine any offset and drift during the course of multiple acquisitions. The WRG (Basi Gas) is supplied as a CO_2–N_2 mixture with a mixing ratio of 0.3538 vol%. The sample inlet system is designed such that it switches automatically between the sample gas and the WRG with an integration time of 320 s. The measurement protocol involves (i) the introduction of the sample gas into the optical multipass cell, which is pre-evacuated and purged with N_2; and (ii) after analysis of the sample, the optical multipass cell is evacuated and purged with N_2 before introducing the WRG. This system is designed and integrated with the TILDAS instrument and controlled using the TDL Wintel software.

The inlet system is constructed using electropolished SS tubes with two different diameters of ¼″ to ½″. It includes electronic valves (Parker, USA), seven pneumatic valves (P9–P15) (Swagelok, USA) for sample gas flow and nitrogen flushing, a capacitance manometer (1000 Torr full scale, MKS, USA), two critical orifices (O'Keefe Controls, USA) and is connected to a dry scroll pump (Agilent, USA) (figure 2). Additionally, an inline particle filter (Swagelok ¼″, SS-4FW-7, 7 Micron) is installed before the sample and nitrogen inlets to prevent contamination of the laser optics, as even tiny particles can significantly increase measurement error.

The analysis involves the introduction of WRG or sample gas in an intermediate volume of approximately 25 ml, which is placed between two critical orifices and pressurized to 600 Torr (figure 2). This gas aliquot is subsequently expanded into the optical multipass cell for measurements (60 Torr cell pressure).

To regulate the flow, 'TDL-Wintel software' employs a predictive model based on a differential equation to determine the closing time of the electronically controlled orifices. It is crucial to introduce the gas slowly to achieve high reproducibility. The WRG cylinder is connected to the system through a critical orifice and solenoid valve S1, while the sample inlet line is connected via a critical orifice and solenoid valve S2 (figure 2).

2.4.3. Instrument stability and precision

Instrument stability was assessed by monitoring the Δ_{638}, δ_{628} and δ_{636} values of the WRG against itself over 6.9 hours (78 acquisitions) at a cell pressure of 60 Torr (figure 3). Each acquisition had an integration time of 320 s. The Allan variance (σ^2) for Δ_{638} decreases over acquisition, following an ideal white noise-limited behaviour, as the measurement progresses and instrumental drift is absent. Instrumental drift influences the δ_{628} and δ_{636} measurements, causing the σ^2 to exceed white noise levels (figure 3). After the 12th acquisition, the standard error for Δ_{638} stabilizes, which led to its selection as the optimal number of acquisitions. The precision of the analytical measurements, expressed as the standard error, is 0.001‰, 0.004‰ and 0.004‰ for Δ_{638}, δ_{628} and δ_{636}, respectively, based on 12 acquisitions (figure 3).

2.5. Data corrections and standardization

2.5.1. Cell pressure correction

The sample and WRG are analysed at a set cell pressure of 60 Torr. However, there exists an offset of −600 to 800 mTorr between the cell pressures for the sample and WRG (figure 4). While most acquisition measurements remain within 0.1% of the target pressure, occasional abrupt fluctuations occur in the WRG pressure. This discrepancy arises from variations in inlet pressure at the critical orifice, which influence the WRG flow rate and, consequently, the timing of the orifice's opening and closing [38]. These differences in cell pressure lead to variation in the peak areas for the sample and WRG, introducing an isotopic shift during the CO_2 analysis [60]. To establish the relationship between the cell pressure offset and shift in isotopic composition, zero enrichment experiments with analysis of the sample and WRG are conducted repeatedly for a long duration (43 acquisitions). A strong linear

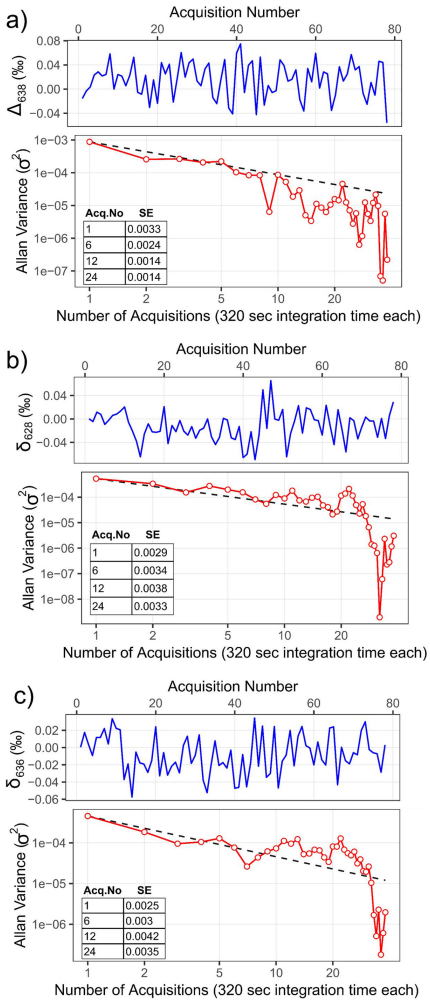

Figure 3. Isotopic values of the WRG were measured against itself (upper panel), and the Allan variance plot (lower panel) shows (a) Δ_{638}, (b) δ_{628} and (c) δ_{636} values over 78 acquisitions at a cell pressure of 60 Torr. The dashed grey line in the lower panel represents white noise. The inset in the lower panel displays the standard error of the isotopic values as a function of the number of acquisitions.

regression (R^2 = 0.931) is observed between Δ_{638} and the cell pressure offset (figure 4). This isotopic effect due to cell pressure offset is corrected using the following equation:

$$\Delta_{638\,\mathrm{Pcorr}} = \Delta_{638\,(\mathrm{raw})} - (\mathrm{m} * \mathrm{P}_{\mathrm{offset}}), \tag{2.3}$$

where $\Delta_{638(\mathrm{raw})}$ denotes the raw isotope values with respect to the WRG, m is the slope of the linear regression and $\mathrm{P}_{\mathrm{offset}}$ is the value of the pressure offset. This correction needs to be applied to different isotopes and to each individual sample that shows a range in pressure offset.

2.5.2. CO_2/N_2 mixing ratio correction

CO_2 was diluted with high-purity N_2 (99.999%) in the TILDAS system to match the WRG concentration of 0.3538 vol%. The disparity in the mixing ratio between the sample analyte's CO_2 and the WRG can lead to differences in the peak area of individual isotopologues of CO_2, which will overall impact measured isotopic values [32,37]. In order to examine the impact of mixing ratio mismatches in the present set-up, a series of experiments with varying bulk isotopic composition of CO_2 is obtained from the digestion of different carbonate reference materials, which include MAR-J1, ETH-1, ETH-2 and ETH-4. These experiments intentionally introduced mixing ratio mismatches at the ppm level while keeping the overall cell pressure constant. The offsets were intentionally extended up to ±400 ppm to constrain the correction across the full operational range of the instrument rather than only near-matched conditions. The experimental observation revealed an insignificant relationship between

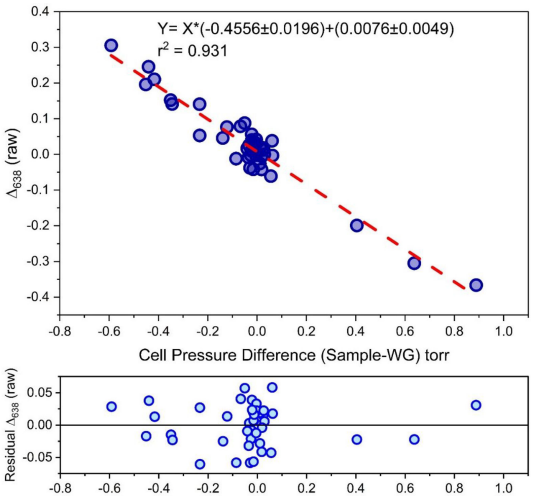

Figure 4. Graphical results for zero enrichment analysis show the relationship between $\Delta_{638(raw)}$ and the pressure offset between the sample and WRG gas analysis. Each data point corresponds to the result of one acquisition.

the mixing ratio (MR) offset and the bulk isotope composition of CO_2 (δ_{638raw}) as well as δ_{628raw}. However, we noted a significant relationship between MR offset and clumped isotope (Δ_{638raw}) and δ_{636raw} (figure 5).

The slope of linear regression (between Δ_{638raw} and MR diff) varies based on the bulk isotope composition of CO_2 (δ_{638raw}). A steeper slope is ascribed to ETH-2 (m = 0.0016 ± 0.0002) and ETH-4 (m = 0.0019 ± 0.0001) (lighter δ_{638raw}), while the slope became shallower for MAR-J1 (m = 0.0009 ± 0.0000) and ETH-1 (m = 0.0008 ± 0.0000) (heavier δ_{638raw}). Subsequently, we formulated a linear York regression model between the mixing ratio regression slope and different bulk isotope compositions of CO_2 (δ_{638raw}), encompassing a range of approximately 29.5‰ (figure 5). This model facilitates the correction of samples with a broad spectrum of bulk isotopic compositions.

$$\text{Mixing ratio regression slope} = (-3.5 \times 10^{-5} \pm 4.5 \times 10^{-6}) * \delta_{638\ \text{Pcorr}} + (0.0019 \pm 0.0001), \tag{2.4}$$

$$\Delta_{638\ \text{MRcorr}} = \Delta_{638\ (\text{Pcorr})} - (\text{Mixing ratio regression slope} * \text{Mixing ratio difference}). \tag{2.5}$$

2.5.3. Role of bulk isotope composition (δ_{628} and δ_{636}) on Δ_{638}

Previous studies have shown an effect of the bulk isotopic composition (δ_{628} and δ_{636}) on Δ_{638} during TILDAS measurements [32,34]. To address this, we performed two sets of experiments on the water–CO_2 exchange at equilibrium temperature of 22°C (allowing them to stay for 48 hours in a temperature-controlled chamber) by (i) changing the water with different $\delta^{18}O$ (range of approximately 20‰), which was expected to yield different δ_{628} post-equilibration and (ii) changing the CO_2 with different $\delta^{13}C$ (covering range from −42.40‰ to +1.97‰). The CO_2 of lighter isotopic composition is obtained from 47 l high-pressure cylinder used as WRG. A heavier isotopic composition is obtained from the acid digestion of MAR-J1. Here, we found a linear relationship between (i) $\Delta_{638\text{-MR}}$ (Δ_{638raw} corrected for mixing ratio) and δ_{628raw} (+0.0087‰$\Delta_{638\text{-MR}}$/1‰ δ_{628raw}) and (ii) $\Delta_{638\text{-MR}}$ and δ_{636raw} (+0.0006‰$\Delta_{638\text{-MR}}$/1‰ $\delta_{636\text{-MR}}$) (figure 6). These linear correlations are subsequently applied to correct sample Δ_{638} using the following equations:

$$\Delta_{638\text{-corrected for }\delta628} = \Delta_{638-\text{MR}} - (+0.0087 * \delta_{628raw}), \tag{2.6}$$

$$\Delta_{638\text{-corrected for }\delta_{636}} = \Delta_{638-\text{MR}} - (+0.0006 * \delta_{636-\text{MR}}). \tag{2.7}$$

2.5.4. Conversion of Δ_{638} to carbon dioxide equilibrium scale reference frame

Clumped isotope data were transferred to the carbon dioxide equilibrium scale (CDES) using equilibrated and heated CO_2 reference gases (CO_2 heated to a stochastic isotopologue distribution at 1000°C) [33]. Two heated gas batches were generated using CO_2 obtained from reacting planktic foraminiferal carbonate from the Bay of Bengal drill core Ocean Discovery Program site 758A. The equilibrated gas was prepared by introducing water with an isotopic value of $\delta^{18}O$ = −13.1‰ relative

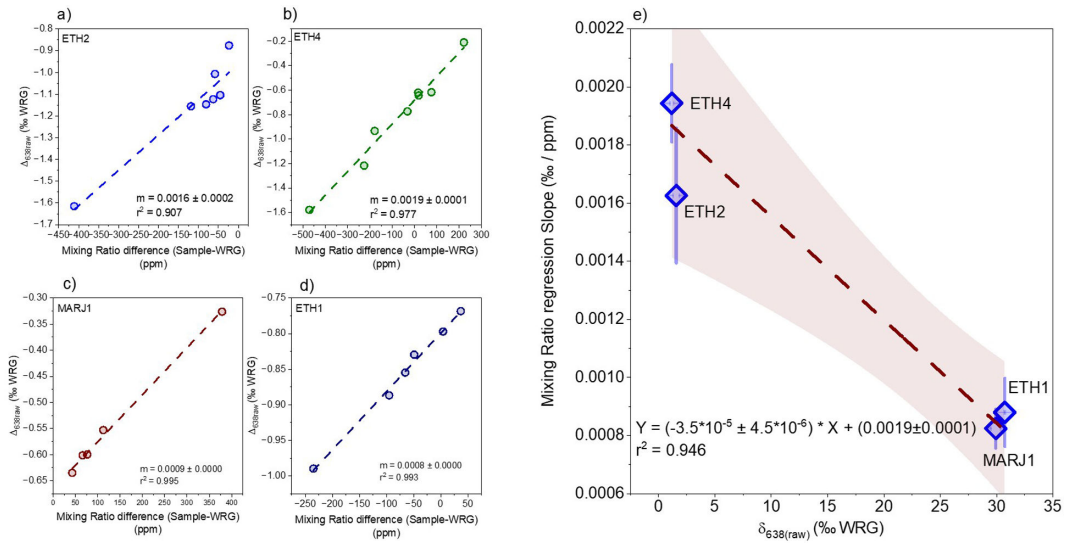

Figure 5. Effect of the mixing ratio difference between the sample and WRG on Δ_{638raw}. (a–d) Relationship between Δ_{638raw} and the mixing ratio difference for ETH2, ETH4, MARJ1 and ETH1. (e) Displays the York linear regression of the mixing ratio regression slope versus δ_{638raw}.

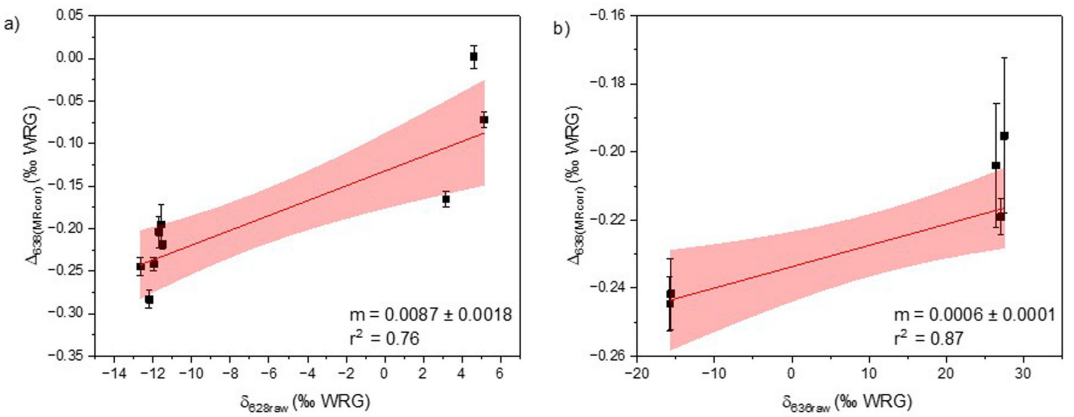

Figure 6. Dependence of Δ_{638} on δ_{628} and δ_{636}. The empirical relationships are shown between $\Delta_{638(MR\ corr)}$ and $\delta_{628(raw)}$ (a) and between $\Delta_{638(MR\ corr)}$ and $\delta_{636(raw)}$ (b) for gases equilibrated at 22°C.

to Vienna standard mean ocean water (VSMOW) into the chamber, followed by freezing of a CO_2 aliquot with $\delta^{13}C = -42.40‰$ relative to Vienna Pee Dee belemnite (VPDB) using liquid nitrogen. The equilibration experiments were performed at 6°C ($n = 3$), 22°C ($n = 7$), 40°C ($n = 1$) and 61°C ($n = 1$) (table 1). The clumped isotope composition (Δ_{638}) measured with respect to WRG using TILDAS is converted to the CDES scale by comparison with its absolute Δ_{638} value predicted theoretically for respective temperatures [29] (figure 7).

2.5.5. Transferring δ_{628} and δ_{636} from the working reference gas scale to the Vienna Pee Dee belemnite scale

Stable isotope ratios (δ_{628} and δ_{636}) measured by TILDAS are referenced to the WRG and were transferred to the VPDB scale using carbonate standards. Primary and secondary standards (NBS-19, IAEA-603, MAR-J1, ETH-1, ETH-2, ETH-3 and ETH-4) were digested at 25°C using the BS method and analysed under identical analytical conditions (table 2). A linear regression was established between the $\delta^{13}C$ and $\delta^{18}O$ values on the VPDB scale, obtained via IRMS [22,23,25,45,61], and the δ_{636} and δ_{628} values on the WRG scale measured with TILDAS (figure 8). This relationship allows for the conversion of sample isotope values from the WRG scale to the VPDB scale.

$$\delta^{13}C\,(‰\ VPDB) = (1.01 \pm 0.01) * \delta_{636}\,(‰\ WRG) + (-26.27 \pm 0.35), \quad (2.8)$$

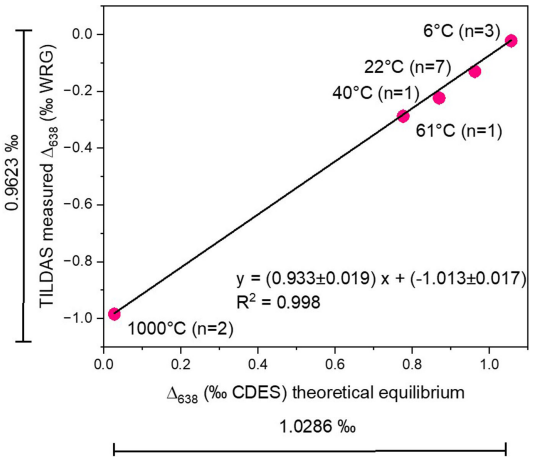

Figure 7. CDES scale conversion. The transfer function for translating the analytical results of Δ_{638} measurements of CO_2 equilibrated with water at different temperatures (6, 22, 40 and 61°C) and CO_2 heated at 1000°C (stochastic CO_2) in the WRG scale to CDES scale using predicted theoretical Δ_{638} values for respective temperature [29]. A replicate number of analyses is indicated in brackets.

Table 1. Clumped isotope (Δ_{638}) values of H_2O-equilibrated CO_2 and heated CO_2 gases on the WRG scale.

s. no.	sample details	temperature (°C)	number of acquisitions	Δ_{638} (‰ WRG)	1 s.e.
1	CO_2 & H_2O equilibration	6	18	−0.0133	0.0108
			31	−0.0323	0.0066
			7	−0.0209	0.0212
	average			−0.0222	
	1 s.d.			0.0096	
	replicates			3	
	1 s.e.			0.0055	
2	CO_2 and H_2O equilibration	22	19	−0.1281	0.0080
			8	−0.0290	0.0131
			9	−0.1079	0.0091
			16	−0.1834	0.0085
			20	−0.1626	0.0055
			18	−0.1250	0.0104
			15	−0.1352	0.0053
			5	−0.1181	0.0184
			10	−0.1110	0.0228
	average			−0.1223	
	1 s.d.			0.0427	
	replicates			9	
	1 s.e.			0.0142	
3	CO_2 and H_2O equilibration	40	19	−0.2235	0.0090
4	CO_2 and H_2O equilibration	61	6	−0.3180	0.0049
5	CO_2 heated gas	1000	4	−0.9900	0.0035
			4	−0.9790	0.0184
	average			−0.9845	
	1 s.d.			0.0078	
	replicates			2	
	1 s.e.			0.0055	

Table 2. Stable isotope values on the WRG scale of primary standards and reference materials digested using the BS method at 25°C.

s. no.	sample details	number of acquisitions	δ_{636} (‰ WRG)	s.d.	1 s.e.	δ_{628} (‰ WRG)	s.d.	1 s.e.
1	MAR-J1	11	27.53	0.04	0.01	5.81	0.06	0.02
		8	27.80	0.04	0.02	5.93	0.06	0.02
	average		27.67			5.87		
	1 s.d.		0.20			0.08		
	replicates		2			2		
	1 s.e.		0.14			0.06		
2	NBS19	11	27.81	0.03	0.01	5.61	0.04	0.01
3	IAEA-603	10	28.27	0.02	0.00	5.37	0.10	0.03
4	ETH-1	17	27.48	0.04	0.01	5.45	0.02	0.01
		7	27.63	0.01	0.00	6.07	0.04	0.01
	average		27.55			5.76		
	1 s.d.		0.10			0.44		
	replicates		2			2		
	1 s.e.		0.07			0.31		
5	ETH-2	12	15.68	0.03	0.01	−10.34	0.04	0.01
		7	15.60	0.01	0.00	−10.36	0.03	0.01
	average		15.64			−10.35		
	1 s.d.		0.06			0.01		
	replicates		2			2		
	1 s.e.		0.04			0.01		
6	ETH-3	15	27.80	0.04	0.01	5.72	0.03	0.01
7	ETH-4	8	15.56	0.04	0.01	−10.64	0.02	0.01
		4	16.41	0.02	0.01	−10.22	0.06	0.03
	average		15.99			−10.43		
	1 s.d.		0.60			0.29		
	replicates		2			2		
	1 s.e.		0.43			0.21		

$$\delta^{18}\mathrm{O}\,(\text{‰ VPDB}) = (1.04 \pm 0.00) * \delta^{628}\,(\text{‰ WRG}) + (-7.97 \pm 0.05)\,. \tag{2.9}$$

2.6. Measurement of water vapour pressure over phosphoric acid

The vapour pressure of H_2O over 104 wt% phosphoric acid was determined using the IAB reaction vessel connected to the CO_2 extraction and cleaning line. The reaction vessel containing phosphoric acid was maintained at designated temperatures of 28, 50, 70, 90 and 110°C. Prior to each measurement, the vessel was held at the target temperature for 10 min to attain thermal equilibrium. Following equilibration, the line was evacuated to establish a baseline pressure, and the headspace pressure was recorded in mBar using a Pfeiffer TPR 280 Compact Pirani Gauge.

2.7. Determination of the 25°C reference value for individual acid bath digestion

For the BS method, isotope values measured at 25°C were directly used as the reference state. In contrast, acid digestion at 25°C using the IAB configuration resulted in unstable gas transfer due to diffusion effects; therefore, measurements were performed at 50, 70 and 90°C only. The 25°C

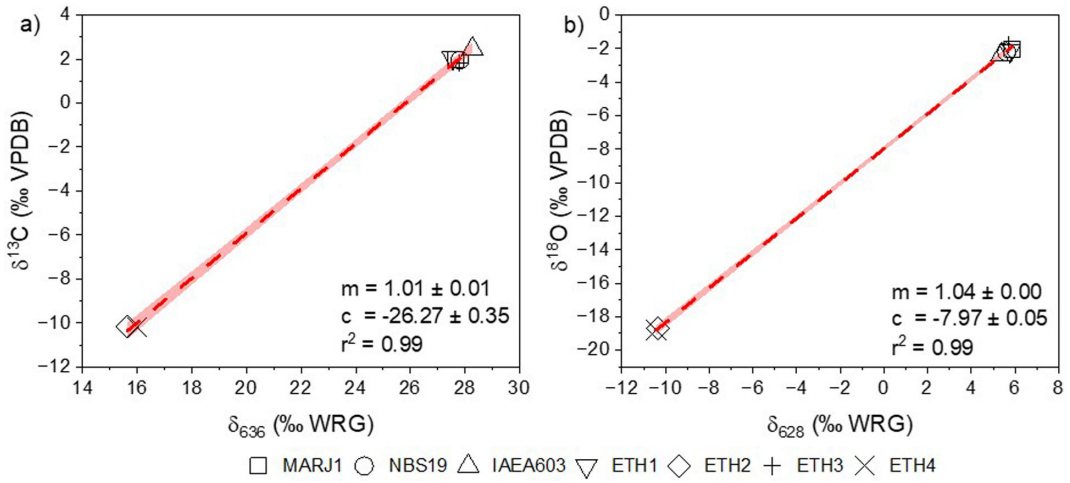

Figure 8. Conversion relationships between WRG and VPDB scales for δ_{636} and δ_{628} measurements. (a) Empirical relationship between $\delta^{13}C$ (‰ VPDB) and δ_{636} (‰ WRG) and (b) $\delta^{18}O$ (‰ VPDB) and δ_{628} (‰ WRG), using accepted values on the VPDB scale [22,23,25,45,61]. The relationships are derived from the analysis of primary standards and reference materials using TILDAS, which are digested in phosphoric acid at 25°C using the BS method. This empirical relationship facilitates the conversion of sample isotope values from the WRG scale to the VPDB scale.

reference values for the IAB method were obtained by extrapolation of the regression defined by the measured temperature-dependent relationship. Weighted least-squares regression accounting for analytical uncertainty was used to determine the temperature dependence, and the value at 25°C was calculated from the fitted function. These extrapolated values were subsequently used to calculate acid fractionation factors for both δ_{628} and Δ_{638}.

3. Results

3.1. Reproducibility of carbonate reference materials

Six reference carbonates (MAR-J1, OMC-J1, ETH-1, ETH-2, ETH-3 and ETH-4) were analysed on a near-daily basis using the IAB digestion method at 90°C (table 3). The measurements remained consistent throughout the analytical session. For MAR-J1 (n = 7), the standard errors for δ_{628}, δ_{636} and Δ_{638} were 0.05‰, 0.02‰ and 0.0134‰, respectively. OMC-J1 (n = 6) yielded 0.14‰, 0.05‰ and 0.0149‰. ETH-1 (n = 6) gave 0.14‰, 0.05‰ and 0.0044‰, whereas ETH-2 (n = 5) produced 0.11‰, 0.04‰ and 0.0248‰. ETH-3 (n = 5) yielded 0.07‰, 0.05‰ and 0.0193‰, and ETH-4 (n = 5) yielded 0.12‰, 0.15‰ and 0.0227‰. Overall, Δ_{638} shows smaller analytical scatter than the corresponding bulk isotope (δ_{628} and δ_{636}) measurements.

3.2. Comparison of Δ_{638} between tunable infrared laser differential absorption spectrometer and isotope ratio mass spectrometer

TILDAS Δ_{638} values on the CDES scale were compared with published IRMS Δ_{47} CDES values for MAR-J1, OMC-J1, ETH reference materials, MERCK and IAEA-C2 at a digestion temperature of 90°C (table 3). The Δ_{638} value obtained for ETH-3 is 0.1921‰ lower than the corresponding Δ_{47} value and was treated as an outlier in the regression analysis (figure 9a). When ETH-3 is excluded, the relationship between TILDAS Δ_{638} and IRMS Δ_{47} yields a slope of 1.0321 ± 0.0425 and an intercept of −0.0433 ± 0.140 (figure 9a).

3.3. Vapour pressure of water over phosphoric acid as a function of temperature

The vapour pressure of H_2O over 104 wt% phosphoric acid was measured at 28, 50, 70, 90 and 110°C using the IAB reaction line (figure 10). The reaction vessel was held at each temperature for 10 min before evacuation and pressure recording. The measured vapour pressure increases exponentially with

Table 3. Summary of δ_{636}, δ_{628} and Δ_{638} values in reference materials using the IAB acid digestion technique at 90°C.

s. no.	reference material	number of acquisitions	δ_{636} (‰ VPDB)	1 s.e.	δ_{628} (‰ VPDB)	1 s.e.	Δ_{638} (‰ CDES)	1 s.e.
1	MAR-J1	12	1.79	0.01	−4.09	0.01	0.3089	0.0104
		13	1.92	0.01	−4.28	0.00	0.2463	0.0115
		16	1.86	0.01	−4.15	0.01	0.3389	0.0076
		13	1.91	0.01	−4.10	0.01	0.2985	0.0082
		10	1.85	0.01	−4.08	0.01	0.3015	0.0105
		4	1.75	0.01	−4.28	0.01	0.3264	0.0032
		8	1.78	0.01	−3.93	0.01	0.3561	0.0093
	average		1.84		−4.13		0.3110	
	1 s.d.		0.07		0.12		0.0353	
	replicates		7		7		7	
	1 s.e.		0.02		0.05		0.0134	
2	OMC-J1	7	−4.85	0.01	−11.55	0.02	0.4147	0.0118
		4	−4.55	0.01	−10.76	0.02	0.4750	0.0198
		6	−4.73	0.01	−11.27	0.02	0.4919	0.0209
		7	−4.76	0.01	−10.67	0.03	0.4534	0.0130
		4	−4.57	0.01	−10.85	0.00	0.4005	0.0068
		9	−4.76	0.01	−10.89	0.01	0.4203	0.0149
	average		−4.70		−11.00		0.4427	
	1 s.d.		0.12		0.34		0.0364	
	replicates		6		6		6	
	1 s.e.		0.05		0.14		0.0149	
3	ETH-1	5	1.83	0.01	−4.56	0.00	0.1589	0.0016
		5	1.85	0.02	−4.53	0.00	0.1590	0.0053
		6	1.65	0.03	−4.31	0.02	0.1526	0.0214
		12	1.70	0.01	−4.77	0.02	0.1791	0.0161
		12	1.73	0.01	−4.75	0.01	0.1758	0.0126
		7	1.55	0.01	−5.35	0.00	0.1723	0.0092
	average		1.72		−4.71		0.1663	
	1 s.d.		0.11		0.35		0.0108	
	replicates		6		6		6	
	1 s.e.		0.05		0.14		0.0044	
4	ETH-2	5	−10.42	0.01	−21.08	0.01	0.2275	0.0062
		6	−10.41	0.01	−21.61	0.02	0.1902	0.0120
		9	−10.46	0.01	−21.32	0.02	0.1019	0.0105
		9	−10.37	0.01	−21.19	0.01	0.1218	0.0097
		8	−10.21	0.02	−21.01	0.03	0.1102	0.0083
	average		−10.37		−21.24		0.1503	
	1 s.d.		0.10		0.24		0.0555	
	replicates		5		5		5	
	1 s.e.		0.04		0.11		0.0248	
5	ETH-3	7	1.82	0.04	−4.27	0.02	0.4351	0.0126

(*Continued.*)

Table 3. (*Continued.*)

s. no.	reference material	number of acquisitions	δ_{636} (‰ VPDB)	1 s.e.	δ_{628} (‰ VPDB)	1 s.e.	Δ_{638} (‰ CDES)	1 s.e.
		14	1.95	0.01	−3.93	0.01	0.3960	0.0101
		9	1.72	0.01	−3.92	0.01	0.4700	0.0102
		13	1.78	0.02	−3.91	0.02	0.3602	0.0119
		12	1.67	0.02	−3.85	0.01	0.4445	0.0096
	average		1.79		−3.98		0.4211	
	1 s.d.		0.10		0.17		0.0432	
	replicates		5		5		5	
	1 s.e.		0.05		0.07		0.0193	
6	ETH-4	7	−10.64	0.01	−21.57	0.01	0.4733	0.0159
		19	−10.34	0.01	−21.94	0.03	0.3349	0.0259
		15	−9.85	0.01	−21.83	0.03	0.4154	0.0215
		11	−10.66	0.02	−21.35	0.02	0.3921	0.0114
		5	−10.47	0.03	−21.35	0.03	0.4279	0.0137
	average		−10.39		−21.61		0.4087	
	1 s.d.		0.33		0.27		0.0508	
	replicates		5		5		5	
	1 s.e.		0.15		0.12		0.0227	
7	MERCK	12	−42.95	0.01	−18.24	0.01	0.4991	0.0097
8	IAEA-C2	7	−8.64	0.01	−11.86	0.02	0.6084	0.0155

temperature. At 90°C, the vapour pressure is approximately 8 times higher than at 28°C, 5.9 times higher than at 50°C and 2.5 times higher than at 70°C (figure 10).

3.4. Relationship between δ_{636} and acid-carbonate reaction temperature

The δ_{636} values show no systematic dependence on acid digestion temperature for either digestion method (figure 11, tables 4 and 5). Across the investigated temperature range, the total variability relative to the mean is approximately 0.4‰.

3.5. Stable oxygen isotope (δ_{628}) acid fractionation factor

The δ_{628} acid fractionation factor varies with digestion temperature for both digestion approaches (figure 12, tables 4 and 5). For the BS method, fractionation is expressed relative to the value measured at 25°C. For the IAB method, the value at 25°C was obtained by extrapolation of the regression defined by measurements at 50, 70 and 90°C. The weighted least-squares regression, accounting for the uncertainty in δ_{628}, for the phosphoric acid fractionation of δ_{628}, is as follows:

(a) BS method:

$$1000\ln \alpha_{\mathrm{dig.temp-25^{\circ}C}} = (0.532 \pm 0.030) \times \frac{10^6}{T^2} + (-6.185 \pm 0.308);\ R^2 = 0.98. \tag{3.1}$$

(b) IAB method:

$$1000\ln \alpha_{\mathrm{dig.\,temp-25^{\circ}C}} = (0.359 \pm 0.027) \times \frac{10^6}{T^2} + (-4.114 \pm 0.247);\ R^2 = 0.97. \tag{3.2}$$

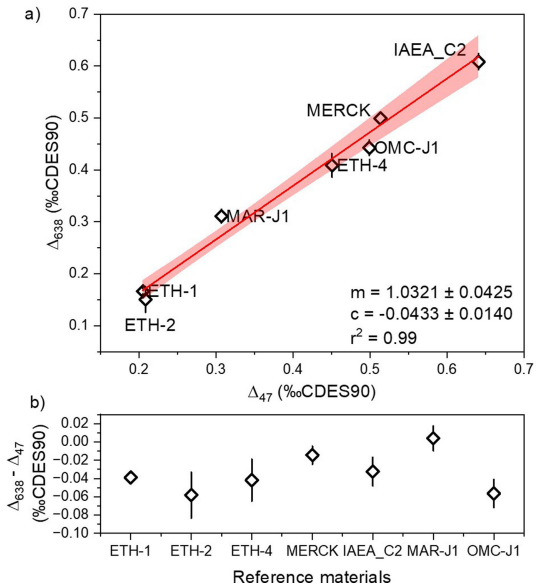

Figure 9. (a) Comparative analysis of Δ_{638} values obtained via TILDAS and Δ_{47} values measured using IRMS for carbonate reference materials at a digestion temperature of 90°C. The Δ_{47} values for ETH-1, ETH-2, ETH-4, MERCK and IAEA-C2 are derived from the InterCarb database [62]. The Δ_{47} values for MAR-J1 and OMC-J1 have been converted from a 25°C acid-carbonate digestion temperature to 90°C using an acid fractionation factor of −0.088‰ [25,29]. ETH-3 is excluded from this analysis due to NO_2 mass interference, which resulted in a Δ_{638} value that is 0.1921‰ lower than the corresponding Δ_{47} value. (b) The difference between the Δ_{638} and Δ_{47} values of reference materials, including propagated error. This discrepancy arises from ^{17}O mass interference, isotope scrambling and pressure baseline effects observed in the IRMS results.

3.6. Clumped isotope (Δ_{638}) acid fractionation factor

The Δ_{638} acid fractionation factor also varies systematically with digestion temperature (figure 13). Fractionation for the BS method is reported relative to the value measured at 25°C, whereas the 25°C value for the IAB method is obtained by extrapolation from higher-temperature measurements. The weighted least-squares regression, accounting for the uncertainty in Δ_{638}, for the phosphoric acid fractionation of Δ_{638} is as follows:

(a) BS method:

$$1000\ln\alpha_{\text{rxn temp}-25^{\circ}\text{C}} = (0.0189 \pm 0.0017) \times \frac{10^6}{T^2} + (-0.2151 \pm 0.0174), \quad R^2 = 0.95. \tag{3.3}$$

(b) IAB:

$$1000\ln\alpha_{\text{rxn temp}-25^{\circ}\text{C}} = (0.0529 \pm 0.0041) \times \frac{10^6}{T^2} + (-0.6072 \pm 0.0356), \quad R^2 = 0.97. \tag{3.4}$$

4. Discussion

4.1. Δ_{638} reference frame and comparison with isotope ratio mass spectrometer Δ_{47} measurements

The CDES provides a reference framework for clumped-isotope measurements by linking measured compositions directly to theoretically predicted equilibrium values and enabling inter-laboratory comparison [33,47]. In recent years, an alternative approach has been adopted in which clumped-isotope data are calibrated using carbonate reference materials with widely accepted Δ_{47} values

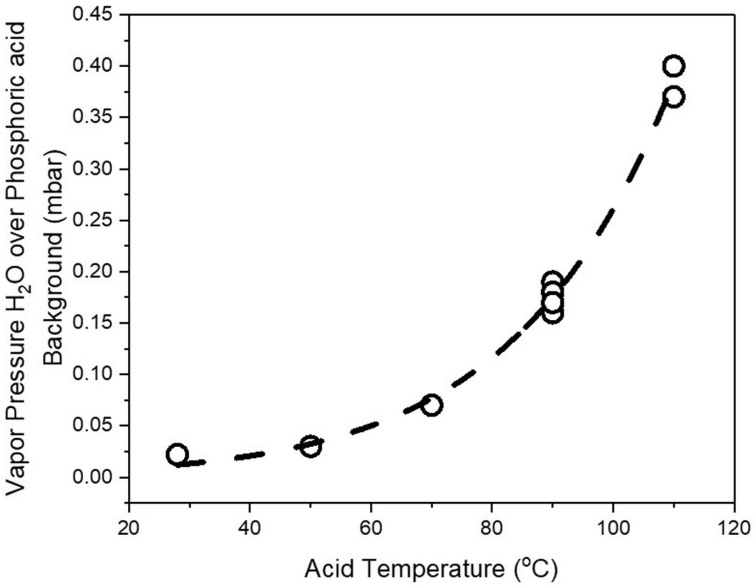

Figure 10. Background vapour pressure of H_2O (mBar) over 104 wt% phosphoric acid at various temperatures for the IAB method.

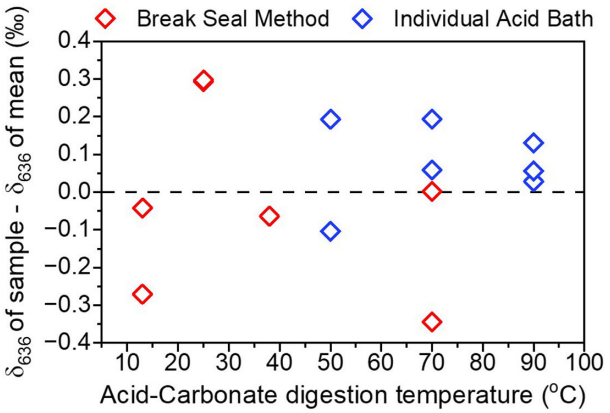

Figure 11. Relationship between δ_{636} and acid-carbonate reaction temperature. Stable carbon isotope (δ_{636}) values for multiple experiments involving both BS method (red open diamond) and IAB (blue open diamond). Data presented as deviation from the mean δ_{636} value of all analyses show minimal effects of reaction temperature on δ_{636}. Standard errors for individual data points range from 0.01 to 0.02‰ (tables 4 and 5).

that are ultimately tied to the gas-based CDES reference frame [62]. This carbonate-based scheme, referred to as Intercarb-CDES (I-CDES), treats standards and unknown samples identically because both are carbonates. However, the available carbonate standards span a narrower compositional and Δ_{47} range than equilibrated gas standards and therefore introduce slightly larger uncertainty [62]. More importantly, absolute Δ_{638} values are not currently established for these carbonate standards, preventing direct application of the I-CDES approach for TILDAS measurements.

In IRMS, the measured quantity Δ_{47} represents a weighted natural-abundance sum of Δ_{638}, Δ_{728} and Δ_{737}, with Δ_{638} dominating the signal, Δ_{728} contributing approximately 3.4% and Δ_{737} being negligible [57]. Because Δ_{728} remains close to zero over a wide temperature range, Δ_{638} is predicted to be approximately 1.0336 times Δ_{47} between 0 and 1000°C, with only minor temperature dependence (1.0273–1.0361) [57]. The relationship obtained in this study between TILDAS Δ_{638} (CDES) and IRMS Δ_{47} (CDES) values (slope 1.0321 ± 0.0425‰; intercept −0.0433 ± 0.140‰) agrees with these theoretical expectations and indicates direct comparability between the two methods (figure 9a). The Δ_{638} CDES value of ETH-3 is 0.1921‰ lower than the corresponding Δ_{47} CDES value, probably reflecting mass interference from NO_2 produced from nitrate during high-temperature acid-carbonate digestion in IRMS measurements [63]. The discrepancy noted between the TILDAS Δ_{638} and IRMS Δ_{47} values can be attributed to factors such as mass interference from ^{17}O, isotope scrambling and baseline pressure effects observed in the IRMS results (figure 9b).

Table 4. Acid fractionation results for stable and clumped isotope analysis of MAR-J1 calcite digested using the BS method (n = number of acquisitions in the analysis).

acid digestion temperature (°C)	$10^6/T^2$ (T in kelvin)	n	Δ_{638} (‰ CDES90)	1 s.e.	1000 ln $\alpha_{\text{dig.temp}-25°C}$ for Δ_{638}	δ_{628} (‰ VPDB)	1 s.e.	1000 ln $\alpha_{\text{dig.temp}-25°C}$ for δ_{628}	δ_{636} (‰ VPDB)	1 s.e.
13	12.21	13	0.4751	0.0093	0.0167	−1.81	0.01	0.21	1.45	0.01
13	12.21	6	0.4552	0.0257	−0.0029	−1.71	0.02	0.31	1.68	0.02
25	11.25	8	0.4494	0.0206	−0.0089	−2.13	0.02	−0.11	2.02	0.02
25	11.25	12	0.4669	0.0165	0.0089	−1.92	0.01	0.11	2.03	0.01
38	10.33	6	0.4372	0.0178	−0.0220	−2.57	0.02	−0.55	1.66	0.01
70	8.49	13	0.4073	0.0155	−0.0532	−3.57	0.01	−1.55	1.73	0.01
70	8.49	8	0.4122	0.0091	−0.0489	−3.70	0.03	−1.67	1.38	0.02
70	8.49	11	0.3971	0.0111	−0.0642	−3.80	0.02	−1.78	1.29	0.01

Table 5. Acid fractionation results for stable and clumped isotope analysis of MAR-J1 calcite digested using the IAB (*n* = number of acquisitions in the analysis).

acid digestion temperature (°C)	$10^6/T^2$ (T in kelvin)	*n*	Δ_{638} (‰ CDES90)	1 s.e.	1000 ln $\alpha_{\text{dig.temp–25°C}}$ for Δ_{638}	δ_{628} (‰ VPDB)	1 s.e.	1000 ln $\alpha_{\text{dig.temp–25°C}}$ for δ_{628}	δ_{636} (‰ VPDB)	1 s.e.
90	7.58	16	0.3368	0.0076	−0.1991	−4.15	0.01	−1.32	1.86	0.01
90	7.58	4	0.3248	0.0032	−0.2111	−4.28	0.01	−1.46	1.75	0.01
90	7.58	8	0.3569	0.0093	−0.1789	−4.28	0.01	−1.45	1.78	0.01
70	8.49	13	0.4074	0.0115	−0.1285	−3.75	0.01	−0.92	1.79	0.02
50	9.58	7	0.4453	0.0066	−0.0905	−3.59	0.01	−0.76	1.62	0.01
50	9.58	6	0.4326	0.0031	−0.1033	−3.48	0.00	−0.65	1.92	0.00
70	8.49	15	0.3742	0.0127	−0.1617	−3.92	0.01	−1.09	1.92	0.01
extrapolated 25	11.25		0.5359			−2.83				

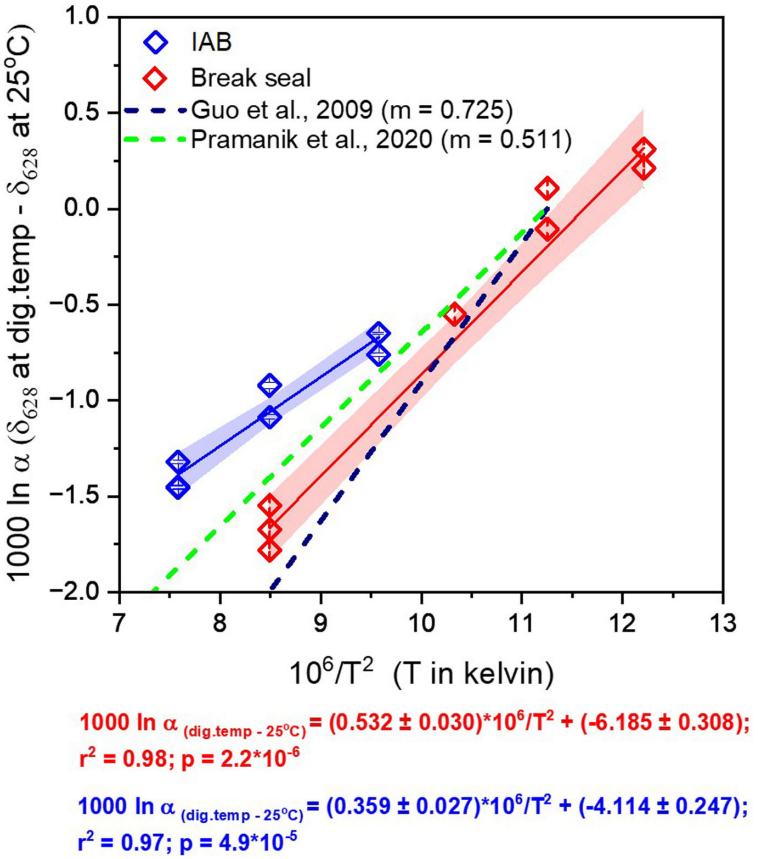

Figure 12. Acid fractionation for oxygen isotopes (δ_{628}). Experimental observation of acid fractionation at different reaction temperatures involving two different acid-carbonate techniques (IAB and BS). Observations are displayed as a deviation of measured δ_{628} values at different acid digestion temperatures from the δ_{628} value documented at 25°C acid-reaction temperature using the BS method (red open diamond). In the case of the IAB (blue open diamond), the 25°C reaction temperature value for δ_{628} is estimated using linear extrapolation of the slope observed from experiments at higher temperatures. The observations are compared with the theoretical acid fractionation lines for δ_{628} species during the acid-carbonate reaction [41,50].

4.2. Mechanism of acid fractionation during carbonate digestion

The temperature dependence observed in both δ_{628} and Δ_{638} indicates that acid fractionation is governed by isotopic exchange between the produced CO_2 and H_2O during phosphoric acid digestion. The source of H_2O is either *in situ* from the phosphoric acid or as a by-product of the acid-carbonate reaction [64]. The vapour pressure measurements performed in this study demonstrate an exponential increase in H_2O vapour pressure with digestion temperature (figure 10). Consequently, isotopic exchange between CO_2 and H_2O becomes progressively more significant at elevated temperatures, whereas it remains limited at low temperatures, where phosphoric acid acts as an efficient water absorbent [8]. The digestion configuration further modulates this behaviour: in the BS approach, CO_2 remains in contact with acid and water throughout the reaction, while in the IAB configuration, CO_2 is continuously removed by cryogenic trapping, restricting equilibration.

The stoichiometry of the acid-carbonate reaction implies complete conversion of carbonate in $CaCO_3$ to CO_2, suggesting no intrinsic isotopic fractionation of δ_{636} with varying acid digestion temperature. However, if CO_2 dissolves in the acid, which commonly occurs in low temperatures and high-viscosity acids, it leads to temperature-dependent isotopic fractionation of δ_{636} [49]. In the present study, no systematic isotopic effect on δ_{636} with changing digestion temperature is observed in either method, discounting the possibility of CO_2 dissolution in the acid (figure 11, tables 4 and 5).

Two reaction pathways can account for this behaviour. One proposed mechanism suggests that the reaction between calcium carbonate and phosphoric acid generates a carbonic acid intermediate without isotopic fractionation, as the reaction is driven to completion before CO_2 collection [41].

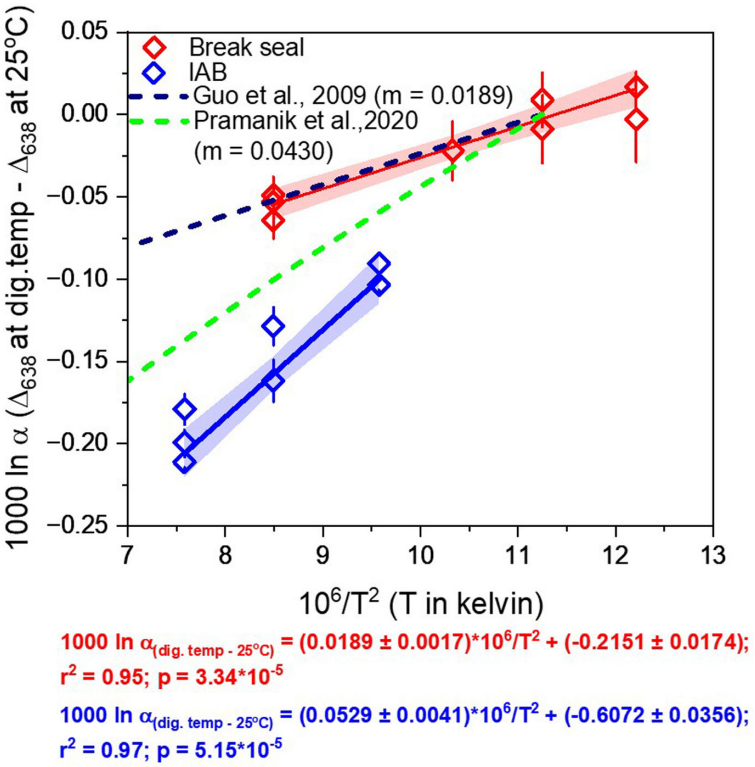

Figure 13. Acid fractionation for carbonate clumped isotope (Δ_{638}) measurements. Comparison of experimental observations of acid fractionation at different reaction temperatures involving two different acid-carbonate techniques. Observations presented here are displayed as a deviation of measured Δ_{638} values at different acid digestion temperatures from the Δ_{638} value documented at 25°C acid-reaction temperature using the BS method (red open diamond). In the case of the IAB (blue open diamond), the 25°C reaction temperature value for Δ_{638} is estimated using linear extrapolation of the slope observed from high-temperature experiments. The observations are compared with the theoretical acid fractionation line for Δ_{638} species during the acid-carbonate reaction [41,50].

Additionally, no isotopic fractionation is anticipated between carbonic acid and phosphoric acid due to the kinetic stability of carbonic acid under anhydrous conditions [41],

$$CaCO_3 + H_3PO_4 \rightarrow CaHPO_4 + H_2CO_3, \tag{4.1}$$

$$H_2CO_3 \rightarrow CO_2 + H_2O\,. \tag{4.2}$$

However, significant isotopic fractionation occurs during the dissociation of carbonic acid into CO_2 and H_2O, owing to the varied dissociation rates of isotopologues and isotopomers. The resulting products, CO_2 and H_2O, undergo partial isotopic exchange until the completion of acid-carbonate digestion [41]. This isotopic exchange mechanism bears a resemblance to the proposed BS method for acid digestion.

Another proposed mechanism for acid-carbonate digestion involves the protonation of carbonate, followed by the immediate removal of CO_2 without any equilibration between the produced CO_2 and H_2O [50]. This pathway corresponds to conditions where exchange is restricted, similar to the IAB digestion method,

$$H_3PO_4 \rightarrow H^+ + H_2PO_4^-, \tag{4.3}$$

$$CaCO_3 + 2H^+ \rightarrow Ca^{2+} + CO_2 + H_2O\,. \tag{4.4}$$

4.3. Temperature dependence of acid fractionation (δ_{628} and Δ_{638})

Both δ_{628} and Δ_{638} exhibit systematic temperature dependence, and the magnitude of fractionation differs between the two digestion methods (figures 12 and 13). For δ_{628}, the slope obtained for MAR-J1 using the BS method (0.532 ± 0.030) closely resembles the slope established using the IRMS approach (0.525) [22], whereas the IAB method yields a shallower relationship (figure 12). In contrast, Δ_{638}

displays the opposite behaviour: the BS configuration produces a shallower slope while the IAB method yields a steeper temperature dependence (figure 13). The slope derived from the BS method using TILDAS is, within uncertainty, identical to the clumped-isotope acid fractionation slope reported for MAR-J1 by IRMS (0.0283) [50].

For δ_{628}, the difference in slope between the BS method and the IAB method reflects the extent of isotope exchange during digestion. In the BS method, the produced CO_2 remains in contact with phosphoric acid and H_2O throughout the reaction, whereas in the IAB method, CO_2 is simultaneously removed from the reaction chamber by cryogenic trapping. Previous experiments demonstrate negligible isotopic exchange at 25°C but substantial exchange at higher temperatures [1,53]. The enhanced exchange at elevated temperature therefore produces a steeper δ_{628} slope for the BS method compared with the IAB configuration.

For Δ_{638}, the behaviour is reversed. The steeper slope of the IAB method indicates that the clumped-isotope composition of the product CO_2 is preserved and not reset by equilibration or reaction intermediates involving free water molecules (figure 13). In contrast, the shallower slope observed in the BS method indicates partial equilibration with water vapour during digestion. The BS method slope closely resembles the theoretical prediction for clumped-isotope acid fractionation (slope = 0.0189), calculated for phosphoric acid digestion proceeding to completion before CO_2 collection and allowing full equilibrium between CO_2 and H_2O [41]. Conversely, the IAB slope approaches the predicted value (0.043) for a reaction dominated by protonation of carbonate with immediate removal of CO_2 and no subsequent equilibration with water [50].

The opposing responses of δ_{628} and Δ_{638}, therefore, arise from how exchange reactions affect bulk and clumped isotopes differently. Increased equilibration modifies oxygen isotopes more strongly, steepening the δ_{628} temperature dependence in the BS configuration, while simultaneously driving Δ_{638} towards equilibrium and reducing its temperature sensitivity. Suppression of equilibration in the IAB method produces the inverse behaviour: a weaker δ_{628} dependence but a stronger Δ_{638} temperature relationship.

The difference between digestion techniques is thus controlled by reaction conditions rather than instrumental behaviour. δ_{628} is referenced to NBS-19 [23,45], whereas Δ_{638} is normalized to stochastic CO_2 [4,57]; consequently, exchange reactions alter the apparent temperature dependence in opposite directions. These observations are consistent with the reaction pathways described in §4.1, in which partial equilibration enhances bulk-isotope modification but diminishes clumped-isotope sensitivity, whereas restricted equilibration preserves kinetic fractionation.

5. Conclusion

This study presents a data reduction technique for TILDAS-based bulk (δ_{628}, δ_{636}) and clumped isotope (Δ_{638}) measurements. Instrumental precision (12 acquisitions of WRG analysed against itself) yields ±0.001‰ (Δ_{638}), ±0.004‰ (δ_{628}) and ±0.004‰ (δ_{636}). Replicate analyses (n = 7) of reference carbonate MAR-J1 achieve external precisions of ±0.013‰ (Δ_{638}), ±0.050‰ (δ_{628}) and ±0.020‰ (δ_{636}). Additionally, this study validates the comparison of TILDAS-based Δ_{638} results with IRMS-based Δ_{47} results, presenting the first calcite acid fractionation factor with varying acid digestion temperature for δ_{628} and acid Δ_{638} for the TILDAS analysis method. It examines two commonly used acid-carbonate digestion methods: the BS method and the IAB method. The study finds no carbon isotope fractionation across different temperatures and digestion methods, ruling out incomplete reactions and acid dissolution effects. The results indicate minimal CO_2 and H_2O equilibration in the IAB method compared with the BS method. These findings are significant as they facilitate inter-laboratory comparison of stable oxygen (δ_{628} or $\delta^{18}O$) and clumped (Δ_{638} or Δ_{47}) isotope ratios in calcite.

Ethics. This work did not require ethical approval from a human subject or animal welfare committee.

Data accessibility. All data necessary for interpretation is provided in tables within the manuscript, with additional Excel files accessible via Zenodo [65].

Declaration of AI use. We have not used AI-assisted technologies in creating this article.

Authors' contributions. T.S.: conceptualization, data curation, formal analysis, funding acquisition, investigation, methodology, visualization, writing—original draft, writing—review and editing; T.K.: funding acquisition, investigation, resources, writing—review and editing; P.G.: conceptualization, supervision, writing—review and editing; D.S.: investigation, writing—review and editing.

All authors gave final approval for publication and agreed to be held accountable for the work performed therein.

Conflict of interest declaration. We declare we have no competing interests.

Funding. We gratefully acknowledge KIT Future Fields funding for the Aerodyne TILDAS. T.S. acknowledges the International Union for Quaternary Research (INQUA) 2023 International Mobility Fellowship, the Grantham Fellowship from DCCC, IISc and the CSIR PhD Fellowship (file no.: 09/079 (2811)/2019-EMR-1).

Acknowledgements. We appreciate the technical support provided by Gesine Preuß, Ralf Wachter and Kevin Altinger. Special thanks to Prof. Stefano Bernasconi and Dr. Heiko Moossen for supplying reference materials and to Dr. William Defliese, Prof. Elisabeth Eiche and Prof. Jochen Kolb for valuable discussions. We thank two anonymous reviewers for their valuable comments that helped refine the manuscript.

References

1. McCrea JM. 1950 On the isotopic chemistry of carbonates and a paleotemperature scale. *J. Chem. Phys*. **18**, 849–857. (doi:10.1063/1.1747785)
2. Kim ST, O'Neil JR. 1997 Equilibrium and nonequilibrium oxygen isotope effects in synthetic carbonates. *Geochim. Cosmochim. Acta* **61**, 3461–3475. (doi:10.1016/S0016-7037(97)00169-5)
3. Schauble EA, Ghosh P, Eiler JM. 2006 Preferential formation of ^{13}C–^{18}O bonds in carbonate minerals, estimated using first-principles lattice dynamics. *Geochim. Cosmochim. Acta* **70**, 2510–2529. (doi:10.1016/j.gca.2006.02.011)
4. Ghosh P, Adkins J, Affek H, Balta B, Guo W, Schauble EA, Schrag D, Eiler JM. 2006 ^{13}C–^{18}O bonds in carbonate minerals: a new kind of paleothermometer. *Geochim. Cosmochim. Acta* **70**, 1439–1456. (doi:10.1016/j.gca.2005.11.014)
5. Kluge T, John CM, Jourdan AL, Davis S, Crawshaw J. 2015 Laboratory calibration of the calcium carbonate clumped isotope thermometer in the 25–250°C temperature range. *Geochim. Cosmochim. Acta* **157**, 213–227. (doi:10.1016/j.gca.2015.02.028)
6. Kluge T, John CM. 2015 Effects of brine chemistry and polymorphism on clumped isotopes revealed by laboratory precipitation of mono- and multiphase calcium carbonates. *Geochim. Cosmochim. Acta* **160**, 155–168. (doi:10.1016/j.gca.2015.03.031)
7. Prasanna K, Ghosh P, Eagle RA, Tripati A, Kapur VV, Feeney RF, Fosu BR, Mishra D. 2021 Temperature estimates of lower Miocene (Burdigalian) coastal water of southern India using a revised otolith 'clumped' isotope paleothermometer. *Geochem. Geophys. Geosyst.* **22**, 1–14. (doi:10.1029/2020GC009601)
8. Defliese WF, Hren MT, Lohmann KC. 2015 Compositional and temperature effects of phosphoric acid fractionation on Δ_{47} analysis and implications for discrepant calibrations. *Chem. Geol*. **396**, 51–60. (doi:10.1016/j.chemgeo.2014.12.018)
9. Zaarur S, Affek HP, Brandon MT. 2013 A revised calibration of the clumped isotope thermometer. *Earth Planet. Sci. Lett*. **382**, 47–57. (doi:10.1016/j.epsl.2013.07.026)
10. Ghosh P, Prasanna K, Banerjee Y, Williams IS, Gagan MK, Chaudhuri A, Suwas S. 2018 Rainfall seasonality on the Indian subcontinent during the Cretaceous greenhouse. *Sci. Rep*. **8**, 1–9. (doi:10.1038/s41598-018-26272-0)
11. Banerjee Y, Thamizharasan S, Ghosh P. 2020 Orbital forcing controlling dry time carbonate precipitation temperature over landmass in the northern mid-latitude during last 50,000 years revealed from carbonate clumped isotope thermometry. *Curr. Sci.* **119**, 265–272. (doi:10.18520/cs/v119/i2/265-272)
12. Eiler JM. 2011 Paleoclimate reconstruction using carbonate clumped isotope thermometry. *Quat. Sci. Rev*. **30**, 3575–3588. (doi:10.1016/j.quascirev.2011.09.001)
13. Kluge T, Affek HP, Dublyansky Y, Spötl C. 2014 Devils Hole paleotemperatures and implications for oxygen isotope equilibrium fractionation. *Earth Planet. Sci. Lett*. **400**, 251–260. (doi:10.1016/j.epsl.2014.05.047)
14. Kluge T *et al*. 2013 Reconstruction of drip-water $\delta^{18}O$ based on calcite oxygen and clumped isotopes of speleothems from Bunker Cave (Germany). *Clim. Past* **9**, 377–391. (doi:10.5194/cp-9-377-2013)
15. Meckler AN *et al*. 2022 Cenozoic evolution of deep ocean temperature from clumped isotope thermometry. *Science* **377**, 86–90. (doi:10.1126/science.abk0604)
16. Sakthivel T, Ghosh P, Bhushan R, Raj H, Dabhi AJ, Shivam A, Senthilnathan D. 2025 Sensitivity of South Asian summer monsoon rainfall to Bay of Bengal sea surface temperature over the past 31 kiloyears. *Glob. Planet. Chang*. **255**, 105118. (doi:10.1016/j.gloplacha.2025.105118)
17. Ghosh P, Garzione CN, Eiler JM. 2006 Rapid uplift of the altiplano revealed through ^{13}C-^{18}O bonds in paleosol carbonates. *Science* **311**, 511–515. (doi:10.1126/science.1119365)
18. Garzione CN, Hoke GD, Libarkin JC, Withers S, MacFadden B, Eiler J, Ghosh P, Mulch A. 2008 Rise of the Andes. *Science* **320**, 1304–1307. (doi:10.1126/science.1148615)
19. Passey BH, Henkes GA. 2012 Carbonate clumped isotope bond reordering and geospeedometry. *Earth Planet. Sci. Lett*. **351–352**, 223–236. (doi:10.1016/j.epsl.2012.07.021)
20. Stolper DA, Eiler JM. 2015 The kinetics of solid-state isotope-exchange reactions for clumped isotopes: a study of inorganic calcites and apatites from natural and experimental samples. *Am. J. Sci*. **315**, 363–411. (doi:10.2475/05.2015.01)
21. Huntington KW, Budd DA, Wernicke BP, Eiler JM. 2011 Use of clumped-isotope thermometry to constrain the crystallization temperature of diagenetic calcite. *J. Sediment. Res*. **81**, 656–669. (doi:10.2110/jsr.2011.51)
22. Ghosh P, Patecki M, Rothe M, Brand WA. Calcite-CO_2 mixed into CO_2-free air: a new CO_2-in-air stable isotope reference material for the VPDB scale. *Rapid Commun. Mass Spectrom.* **19**, 1097–1119. (doi:10.1002/rcm.1886)
23. Coplen TB, Kendall C, Hopple J. 1983 Comparison of stable isotope reference samples. *Nature* **302**, 236–238. (doi:10.1038/302236a0)

24. Epstein S, Buchsbaum R, Lowenstam H, Urey HC. 1951 Carbonate-water isotopic temperature scale. *Geol. Soc. Am. Bull*. **62**, 417. (doi:10.1130/0016-7606(1951)62[417:CITS]2.0.CO;2)
25. Fosu BR, Ghosh P, Mishra D, Banerjee Y, K P, Sarkar A. 2019 Acid digestion of carbonates using break seal method for clumped isotope analysis. *Rapid Commun. Mass Spectrom*. **33**, 203–214. (doi:10.1002/rcm.8304)
26. Huntington KW *et al*. 2009 Methods and limitations of 'clumped' CO_2 isotope (Δ_{47}) analysis by gas-source isotope ratiomass spectrometry. *J. Mass Spectrom.* **44**, 1318–1329. (doi:10.1002/jms.1614)
27. Brand WA, Assonov SS, Coplen TB. 2010 Correction for the ^{17}O interference in $\delta(^{13}C)$ measurements when analyzing CO_2 with stable isotope mass spectrometry (IUPAC Technical Report). *Pure Appl. Chem*. **82**, 1719–1733. (doi:10.1351/PAC-REP-09-01-05)
28. Daëron M, Blamart D, Peral M, Affek HP. 2016 Absolute isotopic abundance ratios and the accuracy of Δ_{47} measurements. *Chem. Geol*. **442**, 83–96. (doi:10.1016/j.chemgeo.2016.08.014)
29. Petersen SV *et al*. 2019 Effects of improved ^{17}O correction on interlaboratory agreement in clumped isotope calibrations, estimates of mineral-specific offsets, and temperature dependence of acid digestion fractionation. *Geochem. Geophys. Geosyst*. **20**, 3495–3519. (doi:10.1029/2018GC008127)
30. Saenger CP, Schauer AJ, Heitmann EO, Huntington KW, Steig EJ. 2021 How ^{17}O excess in clumped isotope reference-frame materials and ETH standards affects reconstructed temperature. *Chem. Geol.* **563**, 120059. (doi:10.1016/j.chemgeo.2021.120059)
31. Huntington KW, Petersen SV. 2023 Frontiers of carbonate clumped isotope thermometry. *Annu. Rev. Earth Planet. Sci*. **51**, 611–641. (doi:10.1146/annurev-earth-031621-085949)
32. Yanay N *et al*. 2022 Rapid and precise measurement of carbonate clumped isotopes using laser spectroscopy. *Sci. Adv*. **8**, eabq0611. (doi:10.1126/sciadv.abq0611)
33. Wang Z, Nelson DD, Dettman DL, McManus JB, Quade J, Huntington KW, Schauer AJ, Sakai S. 2020 Rapid and precise analysis of carbon dioxide clumped isotopic composition by tunable infrared laser differential spectroscopy. *Anal. Chem*. **92**, 2034–2042. (doi:10.1021/acs.analchem.9b04466)
34. Prokhorov I, Kluge T, Janssen C. 2019 Laser absorption spectroscopy of rare and doubly substituted carbon dioxide isotopologues. *Anal. Chem*. **91**, 15491–15499. (doi:10.1021/acs.analchem.9b03316)
35. Prokhorov I, Kluge T, Janssen C. 2019 Optical clumped isotope thermometry of carbon dioxide. *Sci. Rep*. **9**, 4765. (doi:10.1038/s41598-019-40750-z)
36. Crosson ER *et al*. 2002 Stable isotope ratios using cavity ring-down spectroscopy: determination of $^{13}C/^{12}C$ for carbon dioxide in human breath. *Anal. Chem*. **74**, 2003–2007. (doi:10.1021/ac025511d)
37. Bajnai D, Pack A, Arduin Rode F, Seefeld M, Surma J, Di Rocco T. 2023 A dual inlet system for laser spectroscopy of triple oxygen isotopes in carbonate-derived and air CO_2. *Geochem. Geophys. Geosyst*. **24**, 1–13. (doi:10.1029/2023GC010976)
38. Perdue N, Sharp Z, Nelson D, Wehr R, Dyroff C. 2022 A rapid high-precision analytical method for triple oxygen isotope analysis of CO_2 gas using tunable infrared laser direct absorption spectroscopy. *Rapid Commun. Mass Spectrom.* **36**, e9391. (doi:10.1002/rcm.9391)
39. Banerjee S, Ghosh P. 2022 Carbonate clumped isotope analysis using isotope dilution. *Int. J. Mass Spectrom*. **481**, 116916. (doi:10.1016/j.ijms.2022.116916)
40. Sharma T, Clayton RN. 1965 Measurement of ratios of total oxygen of carbonates. *Geochim. Cosmochim. Acta* **29**, 1347–1353. (doi:10.1016/0016-7037(65)90011-6)
41. Guo W, Mosenfelder JL, Goddard WA, Eiler JM. 2009 Isotopic fractionations associated with phosphoric acid digestion of carbonate minerals: insights from first-principles theoretical modeling and clumped isotope measurements. *Geochim. Cosmochim. Acta* **73**, 7203–7225. (doi:10.1016/j.gca.2009.05.071)
42. Kim ST, Mucci A, Taylor BE. 2007 Phosphoric acid fractionation factors for calcite and aragonite between 25 and 75°C: Revisited. *Chem. Geol*. **246**, 135–146. (doi:10.1016/j.chemgeo.2007.08.005)
43. Meckler AN, Ziegler M, Millán MI, Breitenbach SFM, Bernasconi SM. 2014 Long-term performance of the Kiel carbonate device with a new correction scheme for clumped isotope measurements. *Rapid Commun. Mass Spectrom*. **28**, 1705–1715. (doi:10.1002/rcm.6949)
44. Upadhyay D *et al*. 2021 Carbonate clumped isotope analysis (Δ_{47}) of 21 carbonate standards determined via gas-source isotope-ratio mass spectrometry on four instrumental configurations using carbonate-based standardization and multiyear data sets. *Rapid Commun. Mass Spectrom*. **35**, e9143. (doi:10.1002/rcm.9143)
45. Friedman I, O'neil J, Cebula G. 1982 Two new carbonate stable-isotope standards. *Geostand. Newsl*. **6**, 11–12. (doi:10.1111/j.1751-908x.1982.tb00340.x)
46. Ghosh P, Eiler J, Campana SE, Feeney RF. 2007 Calibration of the carbonate 'clumped isotope' paleothermometer for otoliths. *Geochim. Cosmochim. Acta* **71**, 2736–2744. (doi:10.1016/j.gca.2007.03.015)
47. Dennis KJ, Affek HP, Passey BH, Schrag DP, Eiler JM. 2011 Defining an absolute reference frame for 'clumped' isotope studies of CO_2. *Geochim. Cosmochim. Acta* **75**, 7117–7131. (doi:10.1016/j.gca.2011.09.025)
48. Lu C, Murray S, Koeshidayatullah A, Swart PK. 2022 Clumped isotope acid fractionation factors for dolomite and calcite revisited: should we care? *Chem. Geol*. **588**, 120637. (doi:10.1016/j.chemgeo.2021.120637)
49. Swart PK, Burns SJ, Leder JJ. 1991 Fractionation of the stable isotopes of oxygen and carbon in carbon dioxide during the reaction of calcite with phosphoric acid as a function of temperature and technique. *Chem. Geol. Isot. Geosci. Sect*. **86**, 89–96. (doi:10.1016/0168-9622(91)90055-2)
50. Pramanik C, Chatterjee S, Fosu BR, Ghosh P. 2020 Isotopic fractionation during acid digestion of calcite: a combined *ab initio* quantum chemical simulation and experimental study. *Rapid Commun. Mass Spectrom*. **34**, e8790. (doi:10.1002/rcm.8790)

51. Pramanik C, Ghosh P, Banerjee S, Liang M. 2020 *Ab initio* quantum chemical studies of isotopic fractionation during acid digestion reaction of dolomite for clumped isotope application. *Rapid Commun. Mass Spectrom.* **34**, 1. (doi:10.1002/rcm.8926)
52. Böttcher ME. 1996 $^{18}O/^{16}O$ and $^{13}C/^{12}C$ fractionation during the reaction of carbonates with phosphoric acid: effects of cationic substitution and reaction temperature. *Isot. Environ. Health Stud.* **32**, 299–305. (doi:10.1080/10256019608036323)
53. Wachter EA, Hayes JM. 1985 Exchange of oxygen isotopes in carbon dioxide-phosporic acid systems. *Chem. Geol.* **52**, 365–374. (doi:10.1016/0168-9622(85)90046-6)
54. Hillaire-Marcel C, Kim ST, Landais A, Ghosh P, Assonov S, Lécuyer C, Blanchard M, Meijer HAJ, Steen-Larsen HC. A stable isotope toolbox for water and inorganic carbon cycle studies. *Nat. Rev. Earth Environ.* **2**, 699–719. (doi:10.1038/s43017-021-00209-0)
55. Hare VJ, Dyroff C, Nelson DD, Yarian DA. 2022 High-precision triple oxygen isotope analysis of carbon dioxide by tunable infrared laser absorption spectroscopy. *Anal. Chem.* **94**, 16023–16032. (doi:10.1021/acs.analchem.2c03005)
56. Gordon IE *et al*. 2022 The HITRAN2020 molecular spectroscopic database. *J. Quant. Spectrosc. Radiat. Transf.* **277**, 107949. (doi:10.1016/j.jqsrt.2021.107949)
57. Wang Z, Schauble EA, Eiler JM. 2004 Equilibrium thermodynamics of multiply substituted isotopologues of molecular gases. *Geochim. Cosmochim. Acta* **68**, 4779–4797. (doi:10.1016/j.gca.2004.05.039)
58. McManus JB, Nelson DD, Zahniser MS. 2015 Design and performance of a dual-laser instrument for multiple isotopologues of carbon dioxide and water. *Opt. Express* **23**, 6569. (doi:10.1364/oe.23.006569)
59. Tuzson B, Mohn J, Zeeman MJ, Werner RA, Eugster W, Zahniser MS, Nelson DD, McManus JB, Emmenegger L. 2008 High precision and continuous field measurements of $\delta^{13}C$ and $\delta^{18}O$ in carbon dioxide with a cryogen-free QCLAS. *Appl. Phys. B Lasers Opt.* **92**, 451–458. (doi:10.1007/s00340-008-3085-4)
60. Sakai S. 2017 High-precision simultaneous $^{18}O/^{16}O$, $^{13}C/^{12}C$, and $^{17}O/^{16}O$ analyses for microgram quantities of $CaCO_3$ by tunable infrared laser absorption spectroscopy. *Anal. Chem.* **89**, 11846–11852. (doi:10.1021/acs.analchem.7b03582)
61. Bernasconi SM *et al*. 2018 Reducing uncertainties in carbonate clumped isotope analysis through consistent carbonate-based standardization. *Geochem. Geophys. Geosyst.* **19**, 2895–2914. (doi:10.1029/2017GC007385)
62. Bernasconi SM *et al*. 2021 InterCarb: a community effort to improve interlaboratory standardization of the carbonate clumped isotope thermometer using carbonate standards. *Geochem. Geophys. Geosyst.* **22**, 1–25. (doi:10.1029/2020GC009588)
63. Fiebig J *et al*. 2024 Carbonate clumped isotope values compromised by nitrate-derived NO_2 interferent. *Chem. Geol.* **670**, 122382. (doi:10.1016/j.chemgeo.2024.122382)
64. Swart PK, Murray ST, Staudigel PT, Hodell DA. 2019 Oxygen isotopic exchange between CO_2 and phosphoric acid: implications for the measurement of clumped isotopes in carbonates. *Geochem. Geophys. Geosyst.* **20**, 3730–3750. (doi:10.1029/2019GC008209)
65. Sakthivel T, Kluge T, Ghosh P, Stein D. 2024 Acid fractionation during carbonate digestion with phosphoric acid – assessment of two different techniques applied for clumped and stable isotope analysis using a tuneable infrared laser differential absorption spectrometer (TILDAS) [dataset] (Version 1). *Zenodo*. (doi:10.5281/zenodo.13957795)